Special Feature: Popularizing Fuel Cell Vehicles: Designing and Controlling Electrochemical Reactions in the MEA

Research Report

Modeling of Oxygen Transport Resistance in Polymer Electrolyte Fuel Cells

Takahisa Suzuki, Kenji Kudo and Yu Morimoto

Report received on Oct. 16, 2018

ABSTRACT This contribution deals with the oxygen transport resistance in the vicinity of the cathode catalyst-ionomer interface in polymer electrolyte fuel cells (PEFCs). The transport resistance was measured using an ultramicroelectrode coated with a Nafion film less than 100 nm thick, and was resolved into inner (bulk) and interfacial resistances. The films were found to have almost the same inner transport resistivity as a 100 μm thick cast Nafion film. The interfacial resistance was equivalent to 30–70 nm of the Nafion film with only the inner resistance. The existence of a transport barrier at the Pt-Nafion interface was hypothesized. The interfacial transport resistance was included in a model that predicts the performance (current density vs. cell potential) of a membrane-electrode assembly as a pressure-independent transport resistance. The prediction is in agreement with the experimental curve in the intermediate potential region when the pressure-independent resistance is assumed to be potential dependent. The potential dependence suggests that the transport barrier is much thinner than the ionomer film.

KEYWORDS Polymer Electrolyte Fuel Cell, Oxygen Transport, Interfacial Transport Resistance, Thin Ionomer Film, Catalyst Layer

1. Introduction

One of the biggest challenges to achieve the widespread use of polymer electrolyte fuel cell (PEFC) systems is to reduce the amount of electrode catalyst without sacrifice of the performance. This requirement is due to the cost of the catalyst, which is typically made of platinum group metals and accounts for a considerable portion of the cell cost.[1] The voltage penalty in the reduction of catalyst loading often becomes a problem with respect to the oxygen reduction reaction (ORR) at the cathode rather than the hydrogen oxidation reaction (HOR) at the anode because the catalyst activity for the ORR is much lower than that for the HOR. Catalyst loading reduction generally leads to a reduction in the catalyst surface area and leads to an increase in the overall activation loss because the loss is characterized by the specific activity multiplied by the surface area of the catalyst. Reduction of the catalyst surface area is also regarded as a cause of the increase in mass-transport losses because the diffusional flux of reactants increases with a decrease in the catalyst surface area; therefore, the increase in diffusion flux leads to a decrease in the reactant concentration at the catalyst surface.[2-4]

The origin of mass-transport losses has been separately investigated using a model system in which a planar Pt electrode was covered with a Nafion film facing O_2-containing gas.[5-8] The O_2 transport resistance was larger than expected from the bulk diffusion coefficient of Nafion when a very thin film was applied.[9] The O_2 transport resistance could thus be another cause of the observed performance loss in addition to the local increase in the reactant flux with a reduction in catalyst loading. A diffusion barrier was then proposed to be located at the Pt-Nafion and/or Nafion-gas interfaces and the O_2 transport resistance of the barrier was evaluated.

This article first examines the O_2 transport resistance in a model system using a Nafion film with a thickness of 20 nm or less. The experiment reveals the difference between the inner (bulk) and interfacial transport resistance. The performance of a membrane-electrode assembly (MEA) is then predicted with a mathematical model that uses experimentally determined parameters. A potential dependence is introduced to the interfacial transport resistance by fitting the model prediction to the experimental result. The thickness of the diffusion

barrier is then finally estimated using an O_2 transport model inside the barrier.

2. Interfacial Transport Resistance

2. 1 Model

Figure 1 illustrates the steady-state concentration distribution of O_2 in an ionomer (e.g. Nafion) film of thickness x_0 covering a planar Pt electrode at which the ORR occurs. When the diffusion-limited current density is observed, the O_2 concentration at the Pt-ionomer interface (x = 0) is regarded as zero. If there is some type of transport barrier at $x = 0$, then the O_2 concentration just beyond the barrier is larger than zero (denoted c_{Pt}). At $x = x_0$, there is a concentration jump again, assuming another transport barrier, so that the concentration (denoted c_{ion}) is lower than the equilibrium value (denoted c_{eq}). Inside the ionomer film ($0 < x < x_0$), the O_2 flux is assumed to obey Fick's first law. The O_2 flux J_{O_2} can be described as

$$J_{O_2} = -\frac{1}{R_{Pt}} c_{Pt} \qquad (x = 0), \tag{1}$$

$$J_{O_2} = -D\frac{c_{ion} - c_{Pt}}{x_0} \qquad (0 < x < x_0), \tag{2}$$

$$J_{O_2} = -\frac{1}{R_{ion}}\left(c_{eq} - c_{ion}\right) \qquad (x = x_0), \tag{3}$$

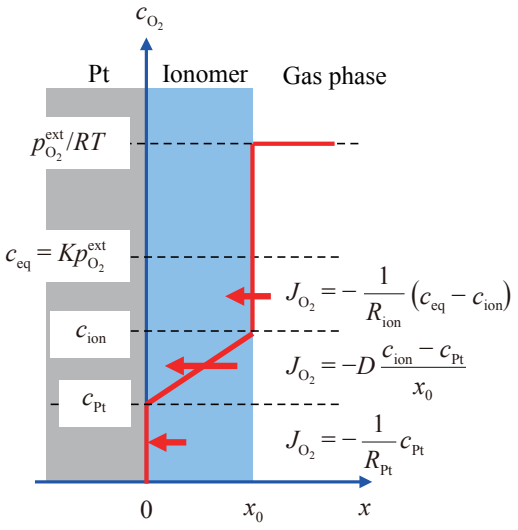

Fig. 1 Schematic of O_2 concentration profile in an ionomer film on a planar Pt electrode.

where R_{Pt} and R_{ion} are the interfacial resistance at the Pt-ionomer and ionomer-gas interfaces, respectively, and D is the diffusion coefficient. The diffusion-limited current density I_d is expressed as

$$I_d = -4F\left|J_d\right|, \tag{4}$$

where F is Faraday's constant. When Henry's law is assumed, c_{eq} is related to the partial pressure of O_2 gas $p_{O_2}^{ext}$ as

$$c_{eq} = Kp_{O_2}^{ext}, \tag{5}$$

where K is Henry's law constant. From Eqs. (1)–(5), the O_2 transport resistance for planar electrode $R_{O_2}^{planar}$ is defined as

$$R_{O_2}^{planar} \equiv \frac{p_{O_2}^{ext}/RT}{\left|I_d\right|/4F} = \frac{1}{RTKD}x_0 + \frac{1}{RTK}\left(R_{ion} + R_{Pt}\right)$$
$$\equiv \rho_{inner}x_0 + R_{interface}. \tag{6}$$

In Eq (6), ρ_{inner} corresponds to the diffusion coefficient inside the film ($0 < x < x_0$), which is called the inner transport resistivity, and $R_{interface}$ corresponds to the barrier at the two interfaces, which is called the interfacial transport resistance.

2. 2 Method

Figure 2 shows a schematic of the cell. The working electrode is a circular cross section of a 10 μm diameter Pt wire sealed in a glass tube. Nafion thin films with various thicknesses were prepared on the electrode from Nafion solution (DE2020, DuPont) diluted with 1-propanol by a solution casting technique. The counter electrode was comprised of a platinized Pt mesh coated with Nafion. The Nafion covering the mesh is in contact with the thin Nafion film coated on the working electrode. These electrodes were placed in a vessel into which humidified O_2-N_2 mixture was flowed. The reference electrode was comprised of a platinized Pt mesh coated with Nafion and was placed in another vessel supplied with humidified 2% H_2-N_2 mixture. A Nafion membrane was used to bridge the Nafion films on the working and reference electrodes. The entire cell was placed in a temperature-controlled convection oven. Cyclic voltammetry was conducted between 0.1 and 1.1 V vs. RHE at a scan rate of

0.1 $V \cdot s^{-1}$. Further experimental details can be found elsewhere.[10]

2. 3 Mechanism

Representative cyclic voltammograms are shown in **Fig. 3**. The red and blue lines show that under N_2 and 1% O_2 atmospheres, respectively. The difference between these two voltammograms, shown in black, includes the ORR current. It does not show an apparent diffusion-limited current, which is often observed in experiments using liquid electrolytes.[11] This is because the diffusion resistance, indicated by the diffusion length divided by the diffusion coefficient, is much larger in liquid electrolytes than in thin Nafion films. In addition, the electrode area effective for the ORR is dependent on the potential because the species that covers the Pt surface, such as sulfonate anions of Nafion, (hydr)oxides, and H atoms, change their coverage depending on potential. The effects from such surface species are determined to be smallest around 0.25 V vs. RHE, and the current at this potential is regarded as the diffusion-limited current.

The inner transport resistivity ρ_{inner} and interfacial transport resistance $R_{interface}$ were determined by fitting the $R_{O_2}^{planar}$ vs. x_0 data to Eq. (6), as shown by the dotted lines in **Fig. 4**. **Figure 5** shows the temperature and relative humidity (RH) dependence of ρ_{inner} and $R_{interface}$. The data for a 100 µm thick Nafion film are also plotted in Fig. 5(a). Both thin (from 20 to 100 nm) and thick (100 µm) films have almost the same inner resistivity, which indicates that the structure that determines the O_2 transport inside Nafion ($0 < x < x_0$) is not affected by the structure of the interfaces ($x = 0$, x_0). The interfacial resistance has different temperature and RH dependence from the inner resistivity, as observed by comparison of Figs. 5(a) and (b). The equivalent film thicknesses of the interfacial resistance, given by $R_{interface}/\rho_{inner}$, were between 30 and 70 nm in the studied temperature and RH ranges. The O_2 flux is predominantly controlled by the interfacial transport resistance when the film is much thinner than the value of $R_{interface}/\rho_{inner}$.

3. Transport Resistance in Catalyst Layers

3. 1 Model

The O_2 transport resistance in an MEA $R_{O_2}^{MEA}$, is formally defined as

$$R_{O_2}^{MEA} \equiv \frac{p_{O_2}^{ext}/RT}{|I_d|/4F}. \quad (7)$$

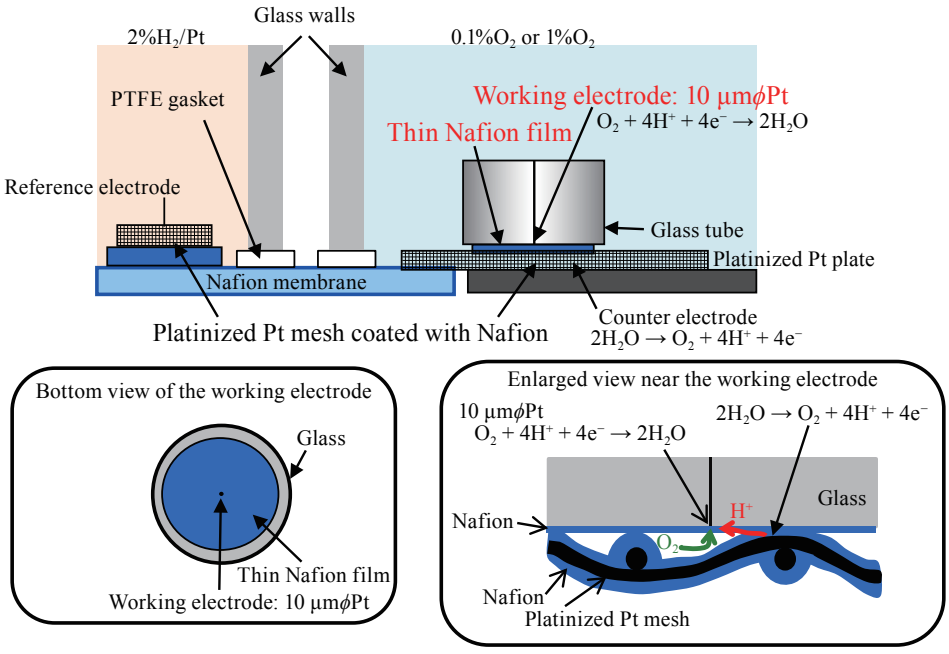

Fig. 2 Geometry of the electrodes.

This includes the diffusion resistance originated from the molecular diffusion through the pores in the gas diffusion layer (GDL) and catalyst layer, as well as the transport resistance from the ionomer surface to the Pt surface. The molecular diffusion coefficient is inversely proportional to the total pressure P; therefore, $R_{O_2}^{MEA}$ can be separated into pressure dependent and independent terms, as

$$R_{O_2}^{MEA} = R_{molec}(P) + R_{other} = R_{molec}^{0} \times \frac{P}{P_0} + R_{other}, \quad (8)$$

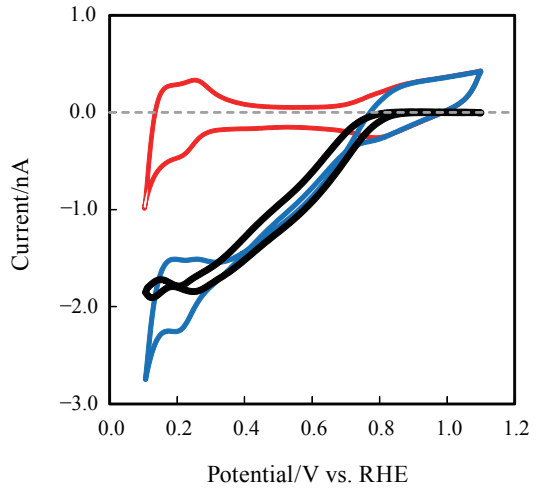

Fig. 3 Cyclic voltammograms of the Pt electrode with 39 nm-thick Nafion film under N_2 (red) and 1% O_2 (blue) atmosphere at 313 K and 60% RH. The black curve is the difference in current between the two conditions.

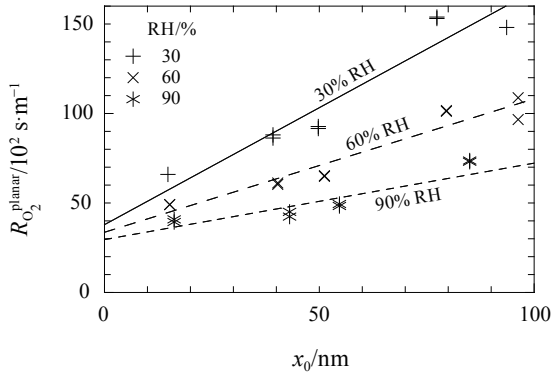

Fig. 4 Oxygen transport resistance for planar electrode $R_{O_2}^{planar}$ planar as a function of Nafion film thickness x_0 at 313 K.

where $R_{molec}(P)$ is the molecular diffusion resistance as a function of P, R_{other} is the pressure independent term, P_0 is the reference pressure, and R_{molec}^{0} is the molecular diffusion resistance at P_0. R_{other} includes the interfacial transport resistance discussed in Sec. 2, and is expressed as

$$R_{other} = \frac{\left(p_{O_2}^{CL} - p_{O_2}(z)\right)/RT}{\left|i_{local}(z)\right|/4F}, \quad (9)$$

where $p_{O_2}^{CL}$ (assumed constant) is the O_2 partial pressure in the pores of the catalyst layer, $p_{O_2}(z)$ (assumed as a function of the distance from the membrane, z) is the equivalent O_2 partial pressure at the Pt-ionomer interface. $i_{local}(z)$ is the local current density described by

$$i_{local}(z) = -i_0 (1 - \theta_{ox}) f \frac{p_{O_2}(z)}{P_0} 10^{-\eta(z)/|b|}, \quad (10)$$

where i_0 is the reference current density, θ_{ox} is the oxide coverage on the Pt surface, f is the roughness

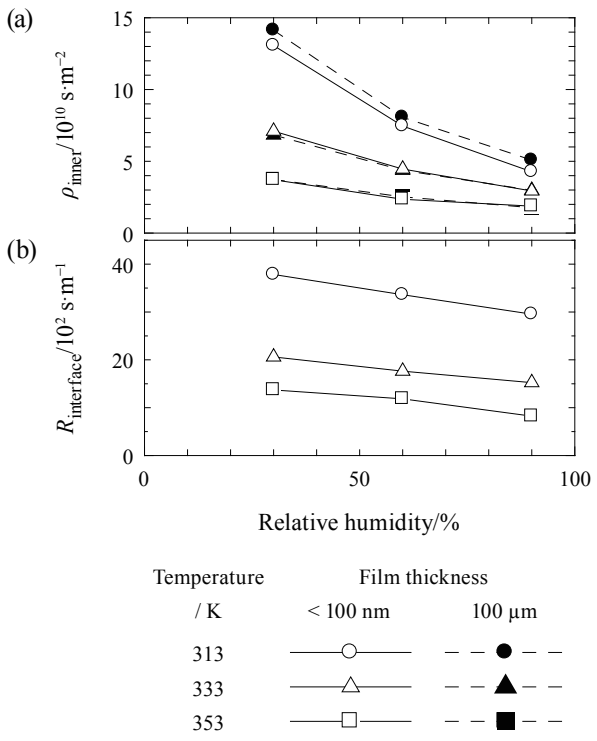

Fig. 5 Inner transport resistivity ρ_{inner} and interfacial transport resistance $R_{interface}$ as a function of relative humidity at different temperatures.

factor of the electrode, η is the overpotential, and b is the Tafel slope.

The MEA performance model deals with the ORR rate distribution in the through-plane direction of the cathode catalyst layer, the ohmic loss in the membrane, and the O_2 concentration decrease in the GDL. The details are available elsewhere.[12] The model is applicable to operating conditions in which moderately and equally humidified gases are supplied at high stoichiometry and the O_2 concentration is sufficiently low. This condition ensures the in-plane homogeneity of the reaction rate, through-plane homogeneity of the water content of the ionomer, and a negligibly small temperature distribution. The value of i_0 was fitted to the experimental data in the high-potential region, and the values of R_{molec} and R_{other} were fitted to the data where I_d was observed (between ca. 0.2 and 0.3 V). Even after fitting the parameters in the model, a significant discrepancy still remained between the model and experimental results[12] in the intermediate potential region, as shown in **Fig. 6**(a). The discrepancy was assumed to be caused by the potential dependence of R_{other}, which includes the interfacial transport resistance. The value of R_{other} was adjusted at each potential so that the model prediction agreed with the experimental result. As the cathode potential increased, the potential dependent R_{other} increased between 0.45 and 0.65 V vs. RHE, and decreased above 0.65 V vs. RHE, as shown in Fig. 6(b).

3. 2 Mechanism

The potential dependence of R_{other} is more likely to be ascribed to the change in the Pt-ionomer interface than that in the ionomer-gas interface because the coverage of the Pt surface species is dependent on the potential. The influence of the decrease in the Pt area with an increase in the potential is considered in the following discussion. If the ionomer covering the Pt is infinitely thin, then $R_{interface}$ discussed in Sec. 2 and the interfacial resistance component in R_{other} would have been inversely proportional to the fraction of the unpoisoned Pt area in the total Pt area. In reality, the ionomer has a finite thickness and hence O_2 diffuses from the ionomer-gas interface that faces the adsorbed species, as well as from that facing the unpoisoned Pt. The situation is shown by a simple 2D model in **Fig. 7**, where the Pt surface is repeatedly covered with adsorbed species at a coverage of θ.

The O_2 concentration profile in the diffusion barrier, which exists in the ionomer, is shown in **Fig. 8** for different aspect ratios of the distance between the unpoisoned Pt sites ($2w$) to diffusion layer thicknesses (t) with the same θ of 0.9. Figure 8(a) shows a contour plot for w = 5 and t = 1. The O_2 concentration is almost uniform above the adsorbed

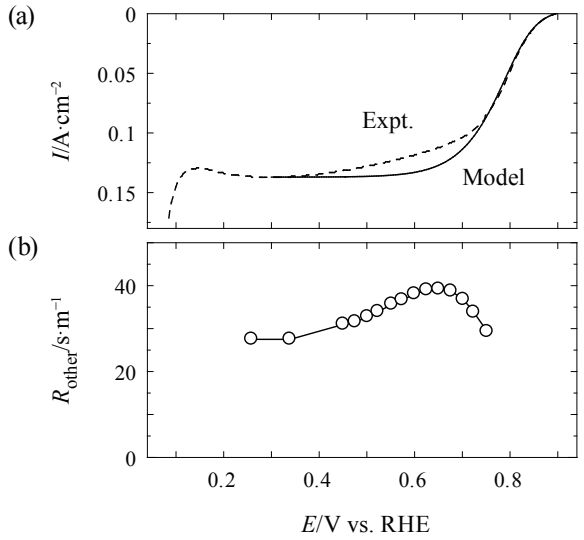

Fig. 6 (a) Comparison of performance curves; dash: experimental, solid: model prediction.
(b) Potential-dependent R_{other} determined so that the model prediction fits the experimental results. E is the cathode electrode potential.

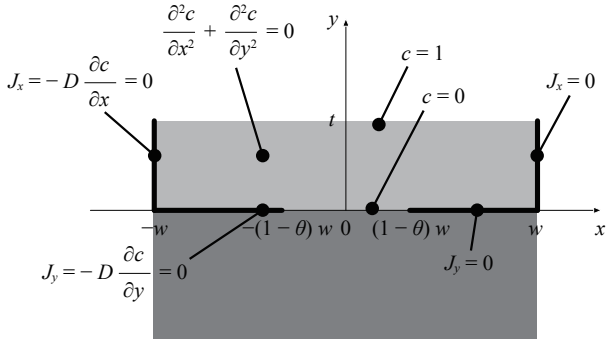

Fig. 7 Ionomer-Pt interface model with equations and boundary conditions that determine the concentration (denoted c) distribution. J_x and J_y are the flux in x and y directions, respectively, and D is the diffusion coefficient.

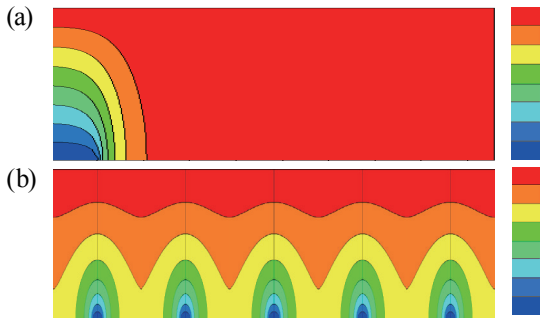

Fig. 8 Oxygen concentration profiles for θ = 0.9. The right color bars correspond to the profiles for θ = 0. Blue: low concentration, red: high concentration. (a) w = 5 and t = 1, and (b) w = 0.5 and t = 1.

species, but in contrast, a regular O_2 concentration gradient is observed above the unpoisoned Pt. This contrast indicates that the O_2 supply to the unpoisoned Pt is mostly through the diffusion layer above unpoisoned Pt. The total O_2 diffusion resistance compared with that for θ = 0 was 5.6. Figure 8(b) shows a contour plot of the O_2 concentration for w = 0.5 and t = 1. In this case, an O_2 concentration gradient is observed over the entire area and O_2 is diffused to unpoisoned Pt through the entire diffusion layer. The total O_2 resistance compared with that for θ = 0 was 1.7, which was less than a third of that in Fig. 8(a). These two examples clearly show that even with an equal coverage, the aspect ratio between the diffusion layer thickness and poisoned area size significantly affects the total diffusion resistance.

With this relation, the thickness of the diffusion barrier can be discussed using θ, w, and t. The value of R_{other} increased by a factor of 1.26 when the potential increased from 0.45 to 0.65 V vs. RHE, as estimated from Fig. 6(b). The coverage at 0.45 V vs. RHE is assumed to be 0.1. If $2w$ = 3 nm (an approximate size of Pt particles) and t = 10 nm (a typical ionomer thickness in catalyst layers) are assumed, then a 1.26 times increase in R_{other} requires θ = 0.9 at 0.65 V vs. RHE. Such a large coverage at 0.65 V is unreasonable, and therefore the diffusion barrier should be much thinner. If $2w$ = 3 nm and t = 1 nm (the thickness of the diffusion barrier predicted by a molecular dynamic simulation[13]) are assumed, in contrast, then θ becomes a moderate value of 0.46 at 0.65 V vs. RHE.

4. Conclusion

The existence of an interfacial transport barrier at a Pt-ionomer interface with a different feature from the bulk ionomer was clarified using a model system of a planar Pt electrode coated with thin Nafion films. The equivalent thickness of the interfacial resistance against the inner resistivity was ca. 30–70 nm. A model for the potential dependent interfacial resistance was proposed by comparing the model prediction for the performance of an MEA with the experimental result. The interfacial resistance increases and then decreases with an increase in the potential. The origin of the increase in the interfacial resistance was discussed using a local diffusion model near the Pt-ionomer interface partially blocked by adsorbed species. The model predicts that the interfacial transport barrier should be thinner than the ionomer that covers the Pt particles in the catalyst layer.

References

(1) Wilson, A., Kleen, G. and Papageorgopoulos, D., "Fuel Cell System Cost - 2017", *DOE Hydrogen and Fuel Cells Program Record* (2017), No. 17007, US Department of Energy.

(2) Nonoyama, N., Okazaki, S., Weber, A. Z., Ikogi, Y. and Yoshida, T., "Analysis of Oxygen-transport Diffusion Resistance in Proton-exchange-membrane Fuel Cells", *J. Electrochem. Soc.*, Vol. 158, No. 4 (2011), pp. B416-B423.

(3) Yoon, W. and Weber, A. Z., "Modeling Low-platinum-loading Effects in Fuel-cell Catalyst Layers", *J. Electrochem. Soc.*, Vol. 158, No. 8 (2011), pp. B1007-B1018.

(4) Hao, L., Moriyama, K., Gu, W. and Wang, C.-Y., "Modeling and Experimental Validation of Pt Loading and Electrode Composition Effects in PEM Fuel Cells", *J. Electrochem. Soc.*, Vol. 162, No. 8 (2015), pp. F854-F867.

(5) Parthasarathy, A., Martin, C. R. and Srinivasan, S., "Investigations of the O_2 Reduction Reaction at the Platinum/Nafion® Interface Using a Solid-state Electrochemical Cell", *J. Electrochem. Soc.*, Vol. 138, No. 4 (1991), pp. 916-921.

(6) Parthasarathy, A., Srinivasan, S., Appleby, A. J. and Martin, C. R., "Temperature Dependence of the Electrode Kinetics of Oxygen Reduction at the Platinum/Nafion® Interface–A Microelectrode Investigation", *J. Electrochem. Soc.*, Vol. 139, No. 9 (1992), pp. 2530-2537.

(7) Parthasarathy, A., Srinivasan, S., Appleby, A. J. and Martin, C. R., "Pressure Dependence of the Oxygen Reduction Reaction at the Platinum Microelectrode/Nafion Interface: Electrode Kinetics and Mass Transport", *J. Electrochem. Soc.*, Vol. 139, No. 10 (1992), pp. 2856-2862.
(8) Kudo, K., Suzuki, T. and Morimoto, Y., "Analysis of Oxygen Dissolution Rate from Gas Phase into Nafion Surface and Development of an Agglomerate Model", *ECS Trans.*, Vol. 33, No. 1 (2010), pp. 1495-1502.
(9) Kudo, K. and Morimoto, Y., "Analysis of Oxygen Transport Resistance of Nafion Thin Film on Pt Electrode", *ECS Trans.*, Vol. 50, No. 2 (2013), pp. 1487-1494.
(10) Kudo, K., Jinnouchi, R. and Morimoto, Y., "Humidity and Temperature Dependences of Oxygen Transport Resistance of Nafion Thin Film on Platinum Electrode", *Electrochim. Acta*, Vol. 209 (2016), pp. 682-690.
(11) Shinozaki, K., Zack, J. W., Richards, R. M., Pivovar, B. S. and Kocha, S. S., "Oxygen Reduction Reaction Measurements on Platinum Electrocatalysts Utilizing Rotating Disk Electrode Technique", *J. Electrochem. Soc.*, Vol. 162, No. 10 (2015), pp. F1144-F1158.
(12) Suzuki, T., Yamada, H., Tsusaka, K. and Morimoto, Y., "Modeling of Oxygen Diffusion Resistance in Polymer Electrolyte Fuel Cells in the Intermediate Potential Region", *J. Electrochem. Soc.*, Vol. 165, No. 3 (2018), pp. F166-F172.
(13) Jinnouchi, R., Kudo, K., Kitano, N. and Morimoto, Y., "Molecular Dynamics Simulations on O_2 Permeation through Nafion Ionomer on Platinum Surface", *Electrochim. Acta*, Vol. 188 (2016), pp. 767-776.

Fig. 1
Reprinted and modified from Electrochim. Acta, Vol. 209 (2016), pp. 682-690, Kudo, K., Jinnouchi, R. and Morimoto, Y., Humidity and Temperature Dependences of Oxygen Transport Resistance of Nafion Thin Film on Platinum Electrode, © 2016 Elsevier, with permission from Elsevier.

Figs. 2 and 3
Reprinted from Electrochim. Acta, Vol. 209 (2016), pp. 682-690, Kudo, K., Jinnouchi, R. and Morimoto, Y., Humidity and Temperature Dependences of Oxygen Transport Resistance of Nafion Thin Film on Platinum Electrode, © 2016 Elsevier, with permission from Elsevier.

Figs. 6-8
Reprinted from J. Electrochem. Soc., Vol. 165, No. 3 (2018), pp. F166-F172, Suzuki, T., Yamada, H., Tsusaka, K. and Morimoto, Y., Modeling of Oxygen Diffusion Resistance in Polymer Electrolyte Fuel Cells in the Intermediate Potential Region.

Takahisa Suzuki
Research Fields:
- Polymer Electrolyte Fuel Cells
- Electrochemistry

Academic Societies:
- The Electrochemical Society
- The Physical Society of Japan

Kenji Kudo
Research Field:
- Slurry for Catalyst Layer of Polymer Electrolyte Fuel Cells

Academic Degree: Dr. Eng.
Academic Society:
- The Electrochemical Society of Japan

Award:
- Excellent Paper Award, The Electrochemical Society of Japan, 2006

Yu Morimoto
Research Fields:
- Electrochemical Devices
- Fuel Cells

Academic Degree: Ph.D
Academic Societies:
- The Electrochemical Society
- The Electrochemical Society of Japan

